

REGULAR PAPERS

Nanowire size dependence on sensitivity of silicon nanowire field-effect transistor-based pH sensor

To cite this article: Ryoongbin Lee *et al* 2017 *Jpn. J. Appl. Phys.* **56** 124001

View the [article online](#) for updates and enhancements.

Related content

- [Investigation of drift effect on silicon nanowire field effect transistor based pH sensor](#)
Sihyun Kim, Dae Woong Kwon, Ryoongbin Lee *et al.*
- [Optimized operation of silicon nanowire field effect transistor sensors](#)
Taiuk Rim, M Meyyappan and Chang-Ki Baek
- [Experimental Characterization of Quasi-Fermi Potential Profile in the Channel of a Silicon Nanowire Field-Effect Transistor with Four-Terminal Geometry](#)
Soshi Sato, Kenji Ohmori, Kuniyuki Kakushima *et al.*



Nanowire size dependence on sensitivity of silicon nanowire field-effect transistor-based pH sensor

Ryongbin Lee¹, Dae Woong Kwon¹, Sihyun Kim¹, Sangwan Kim², Hyun-Sun Mo³, Dae Hwan Kim³, and Byung-Gook Park^{1*}

¹Inter-university Semiconductor Research Center (ISRC) and Department of Electrical and Computer Engineering, Seoul National University, Seoul 08826, Republic of Korea

²Department of Electrical and Computer Engineering, Ajou University, Suwon 16499, Republic of Korea

³School of Electrical Engineering, Kookmin University, Seoul 02707, Republic of Korea

*E-mail: bgpark@snu.ac.kr

Received March 10, 2017; revised September 6, 2017; accepted September 12, 2017; published online November 20, 2017

In this study, we investigated the effects of nanowire size on the current sensitivity of silicon nanowire (SiNW) ion-sensitive field-effect transistors (ISFETs). The changes in on-current (I_{on}) and resistance according to pH were measured in fabricated SiNW ISFETs of various lengths and widths. As a result, it was revealed that the sensitivity expressed as relative I_{on} change improves as the width decreases. Through technology computer-aided design (TCAD) simulation analysis, the width dependence on the relative I_{on} change can be explained by the observation that the target molecules located at the edge region along the channel width have a stronger effect on the sensitivity as the SiNW width is reduced. Additionally, the length dependence on the sensitivity can be understood in terms of the resistance ratio of the fixed parasitic resistance, including source/drain resistance, to the varying channel resistance as a function of channel length. © 2017 The Japan Society of Applied Physics

1. Introduction

As interest in point-of-care (PoC) testing has grown, rapid, sensitive, and equipment-free diagnoses have become important. Following these trends, biosensors based on ion-sensitive field-effect transistors (ISFETs) have been widely studied owing to their label-free, highly sensitive, and real-time detection of biological entities such as DNA, viruses, and proteins. A number of studies of sensing various target molecules have been reported.^{1–5} Furthermore, ISFET sensors with CMOS-compatible device structures have received considerable attention owing to their good uniformity, high reproducibility, and low-cost fabrication for mass production.^{6–13} The principle of electrical detection by ISFET sensors is based on the gating effect of the charged biomolecules on the gate oxide, which can be converted directly to changes in electrical properties such as current, conductance, and threshold voltage.^{14–16} Beginning with micrometer-scale ISFET devices,^{17–19} various researchers have reported achieving the maximum sensitivity of ISFETs.^{20,21} In recent years, silicon nanowire (SiNW) channels^{1–4,6–13} and carbon nanotubes (CNTs)²² have been studied to improve their sensing performance due to their high gate controllability and surface-to-volume ratio. In terms of sensing performance, sensitivity is defined as relative conductance or current change, which is strongly related to the intrinsic performance of SiNW FETs. The relationship between nanowire size and sensitivity has been studied in various types of SiNW ISFETs.^{23–25} It is broadly accepted that SiNW ISFETs with a small cross section tend to have higher sensitivity. However, the effect of enhancing surface-to-volume ratio on the sensitivity of SiNW ISFETs has not yet been specifically investigated by using fabricated SiNW ISFETs. Moreover, it is necessary to consider the physical effect of the nanowire structure on sensitivity owing to the electric field concentration from the edges of the nanowire as the width decreases. In terms of length dependence on sensitivity, rigorous analysis has not been possible owing to insufficient experimental results.

Our group has developed a SiNW biosensor that can be completely integrated with CMOS readout circuits.^{26,27} In

this study, we examined its sensitivity using fabricated SiNW ISFET-based pH sensors of various lengths and widths. On the basis of experimental results, the sensitivity depending on nanowire size was explained. Through technology computer-aided design (TCAD) simulations, the physical backgrounds of the width/length-dependent sensitivity were rigorously investigated.

2. Experiment procedure and simulation conditions

2.1 Fabrication and experiment procedure

We fabricated a SiNW ISFET with a liquid gate for pH detection. The details of the fabrication are illustrated in Fig. 1(a). Firstly, n/p-channel regions are defined by ion implantation. A B^+ dose of $7 \times 10^{12} \text{ cm}^{-2}$ and 20 keV are applied to the n-channel region, whereas a P^+ dose of $3 \times 10^{13} \text{ cm}^{-2}$ and 40 keV are applied to the p-channel region. SiNW active regions are formed by an electron-beam (e-beam) mix-and-match lithography process followed by dry etching. After gate oxidation for the gate dielectric and the deposition of the poly-Si gate for MOSFETs in CMOS readout circuits, poly-Si on the nanowire channels of the ISFETs are etched by the reactive-ion-etching (RIE) process in HBr/O_2 gas. Source and drain regions is implanted with As^+ ($3 \times 10^{15} \text{ cm}^{-2}$) in n-channel devices and BF_2^+ ($3 \times 10^{15} \text{ cm}^{-2}$) in p-channel devices, respectively. Then, the conventional back-end-of-line (BEOL) process is conducted. An interlayer dielectric (ILD) is deposited with oxide by the high-density plasma chemical vapor deposition (HDPCVD) process. Next, contact hole etching and metallization are carried out to wire the sensors and their readout circuits. Lastly, the sensing area is opened by oxide etching process in CHF_3/CF_4 plasma. The schematics of the fabricated SiNW ISFET are shown in Figs. 1(b) and 1(c). The device structure is similar to the conventional SiNW MOSFET structure, except that the SiNW channel is opened to contact a pH solution to which a liquid gate voltage is applied. Scanning electron microscopy (SEM) and transmission electron microscopy (TEM) images of the fabricated SiNW sensor are shown in Fig. 2. Figure 2(a) indicates that the SiNW sensor is fabricated adequately and the sensing area is opened successfully.

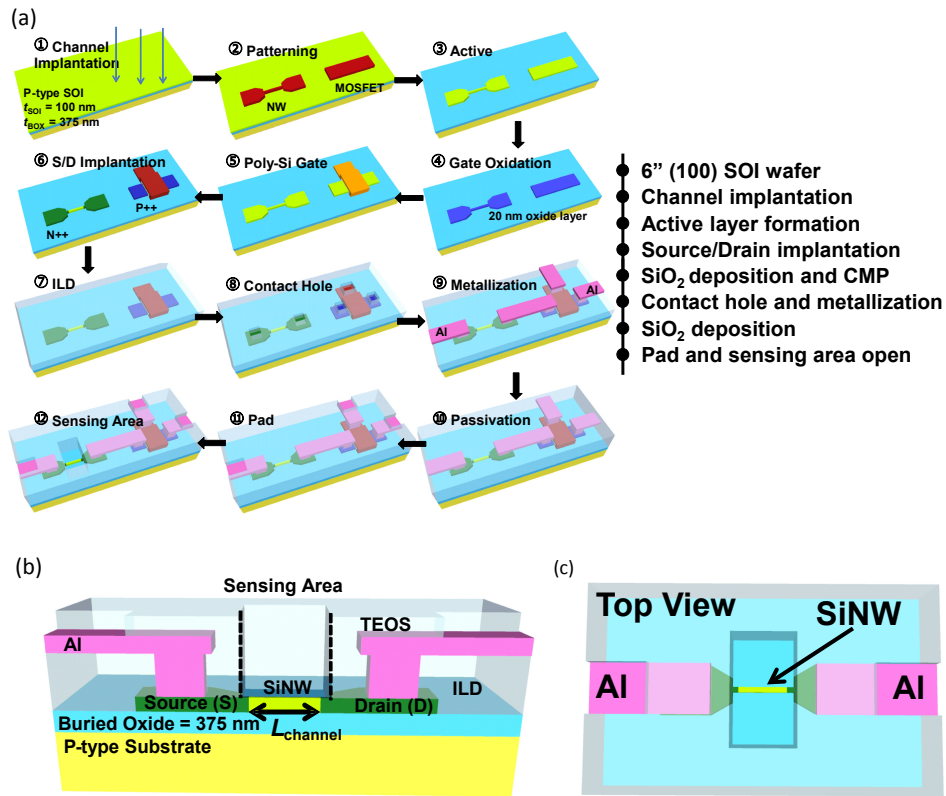


Fig. 1. (Color online) Schematic illustration of (a) fabrication procedure and (b) cross-sectional and (c) top views of SiNW ISFET.

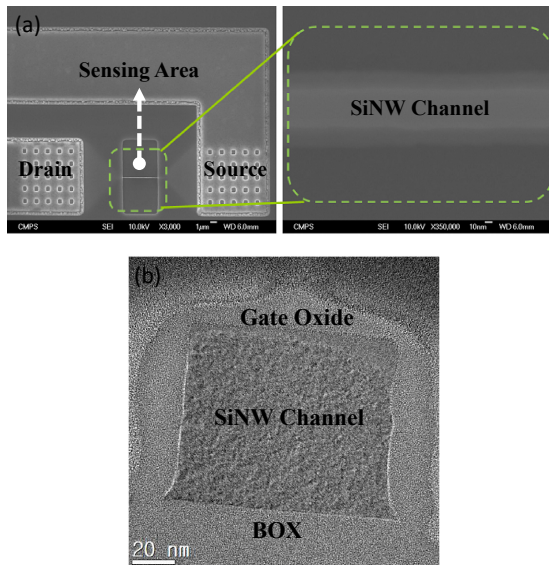


Fig. 2. (Color online) (a) SEM images of SiNW ISFET and (b) cross-sectional TEM image of SiNW.

Figure 2(b) shows that the corners of the Si channel are slightly round, so the effective SiNW width becomes smaller because the liquid gate potential can be applied more deeply at the corners of the channel. Thus, the sensitivity is enhanced in SiNWs with rounded corners, compared with SiNWs with right-angled corners in the simulated device structure. Furthermore, the SiNW channel and the gate oxide of the sensor are preserved during the etching of the sensing area, as shown in Fig. 2(b). The width and thickness of the SiNW are 105 and 80 nm, respectively. The measurement procedure is illustrated in Fig. 3. Poly(dimethylsiloxane) (PDMS) is attached to the fabricated chip.

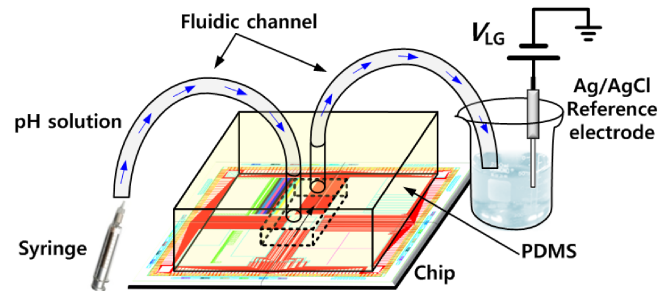


Fig. 3. (Color online) Schematic diagram of measurement setup.

oxide surface of the SiNW sensor is functionalized using 3-aminopropyl-triethoxysilane (APTES) to obtain an amine ($-\text{NH}_2$) surface. An amine surface is used to maintain the linearity of sensitivity from low to high pH values of the pH solution.¹⁴⁾ The SiO₂ surface of the SiNW is treated with 0.1× potassium phosphate buffer solutions with three different pHs (pHs 4, 7, and 10) to detect H⁺ or OH⁻ ions. A fluidic channel is used to inject the pH solution. Liquid gate bias is applied to the pH solution through the Ag/AgCl reference electrode.

2.2 TCAD simulation conditions

TCAD simulations are conducted to analyze the physical origin of pH sensitivity in the SiNW sensors. The details of the TCAD simulation method are described in a previous report.²⁸⁾ The device architecture and physical parameters of the SiNW sensor used in this work are shown in Fig. 4 and Table I, respectively. The channel length of the SiNW is 2 µm. The source and drain regions are doped with $2 \times 10^{20} \text{ cm}^{-3}$ arsenic and the channel doping concentration is $1 \times 10^{17} \text{ cm}^{-3}$ (boron). In addition, we consider that the electrical double layer is a dielectric layer with a thickness of 4.43

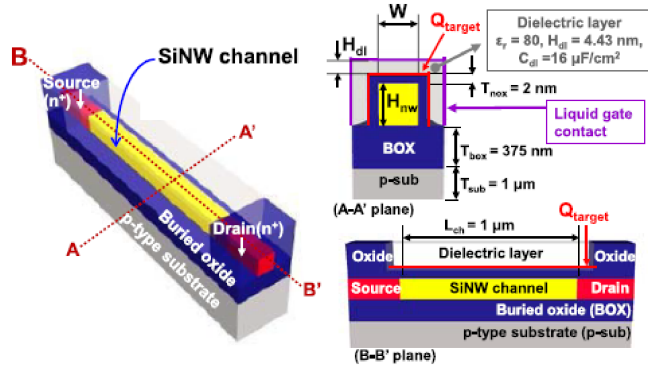


Fig. 4. (Color online) Device structure of SiNW ISFET used in simulations.

Table I. Parameters used in these simulations.

Parameter	Value
NW width (nm)	35, 60, 300
NW length (μm)	2
Oxide thickness T_{ox} (nm)	2
NW thickness H_{nw} (nm)	80
Double layer thickness H_{dl} (nm)	4.43
Box thickness T_{box} (nm)	375
S/D doping (cm^{-3})	$Ar \ 2 \times 10^{20}$
Channel doping (cm^{-3})	$B \ 1 \times 10^{17}$

nm.¹⁴) H^+ and OH^- ions are modeled as positive and negative charges on the gate oxide. The site-binding theory is used to model the sensing mechanisms of target molecules with charges.²⁹) All the simulations are conducted using a Synopsys Sentaurus™ TCAD simulator.

3. Results and discussion

3.1 Width dependence on sensitivity of SiNW sensor

Figure 5 shows the transfer curves of the ISFETs of 35, 60, 70, 120, and 300 nm widths measured at pH 7. The threshold voltage of each ISFET is slightly different and thus the sensitivity is defined at a fixed gate overdrive voltage (0.2 V) to allow comparison between devices. Threshold voltages are extracted from the transfer curves by the linear extrapolation method.³⁰) As a result, in Fig. 5, the threshold voltages of the ISFETs are 1.05, 1, 1, 0.97, and 0.8 V.

Figure 6(a) shows the changes in the transfer curve as a function of pH and Fig. 6(b) shows the width dependence of the relative current change (sensitivity; $\Delta I_{ON}/I_{ON}$ at pH 7) extracted from the transfer curves. In Fig. 6(a), as pH increased, more negative charges (OH^- ions) are bound on the gate oxide of the SiNW ISFET. Thus, the transfer curve is shifted to the right and I_{ON} is decreased at a fixed liquid gate voltage. Figure 6(b) indicates that the SiNWs with smaller widths tend to have higher sensitivity. In general, the absolute I_{ON} and ΔI_{ON} are both reduced as the nanowire width decreases. However, in relative terms, $\Delta I_{ON}/I_{ON}$ is improved as the nanowire becomes narrower. The simulated $\Delta I_{ON}/I_{ON}$ data in Fig. 7 are also consistent with the measurement results. This tendency can be explained by the fact that the electron concentration of a narrower nanowire increases more sharply than that of a wider nanowire. To understand the width dependence on the sensitivity of SiNW, one needs to focus on two factors: surface-to-volume ratio and e-field concentration. E-field concentration means that both the

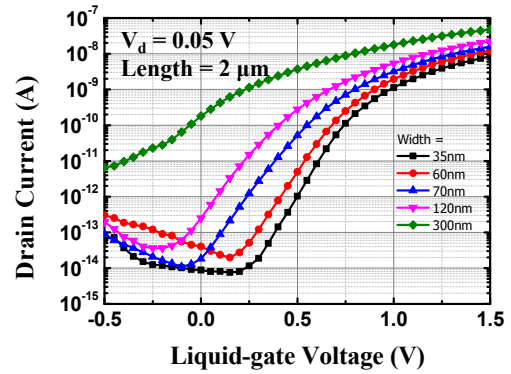


Fig. 5. (Color online) Transfer curves of n-type SiNW ISFETs of various widths at pH 7.

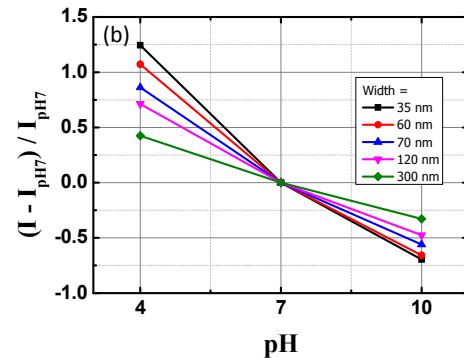
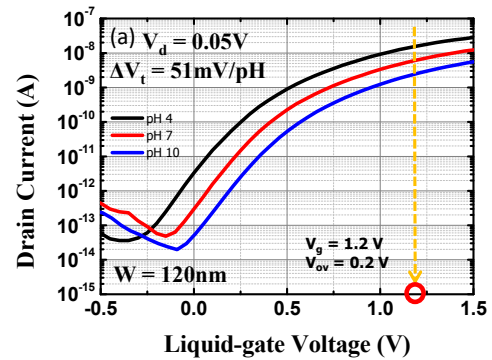


Fig. 6. (Color online) (a) I_{ON} extraction of n-type SiNW pH sensor and (b) I_{ON} sensitivity of ISFETs of various widths as a response to pH change.

vertical and lateral e-fields affect the electrostatic potential of the channel, especially at the corners of the nanowire. Figure 8 shows that the energy band is more bent at the corners owing to the combination of the e-fields crowding in both directions. Owing to the additional band bending, the electron density at the corners is higher than that in the middle. Figure 9 shows the simulated electron density (e-density) of the SiNW across the channel width and Fig. 10 shows that the relative increase in the number of electrons (the ratio of electron concentration at pHs 4 and 10 at the same V_{ov}) in the entire SiNW area is largest in the 35 nm SiNW. Interestingly, the sensitivity change increases markedly when the nanowire width becomes sub-60 nm, as shown in Fig. 11(a). This is because the mechanism of sensitivity enhancement is slightly different between the narrow and wide SiNWs. When the SiNW is wider (over 60 nm), the sensitivity depending on the decreased SiNW width is generally improved by the decrease in the area of the channel region where the e-field is not con-

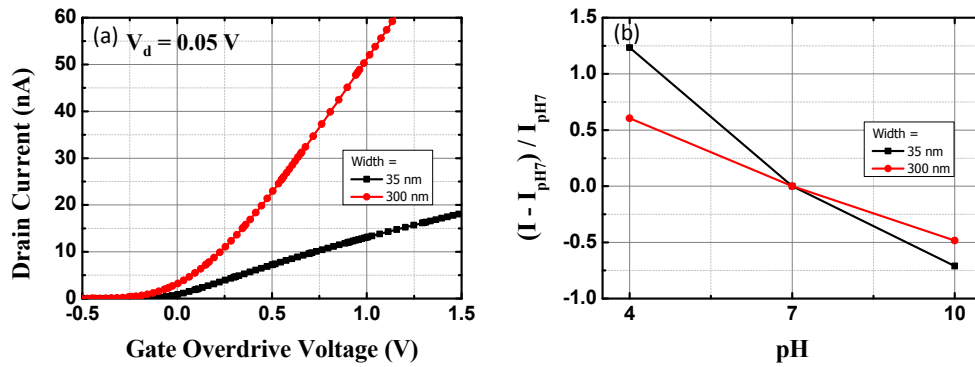


Fig. 7. (Color online) Simulated (a) transfer curves and (b) $\Delta I_{ON}/I_{ON}$ in the 35- and 300-nm-width SiNW ISFETs.

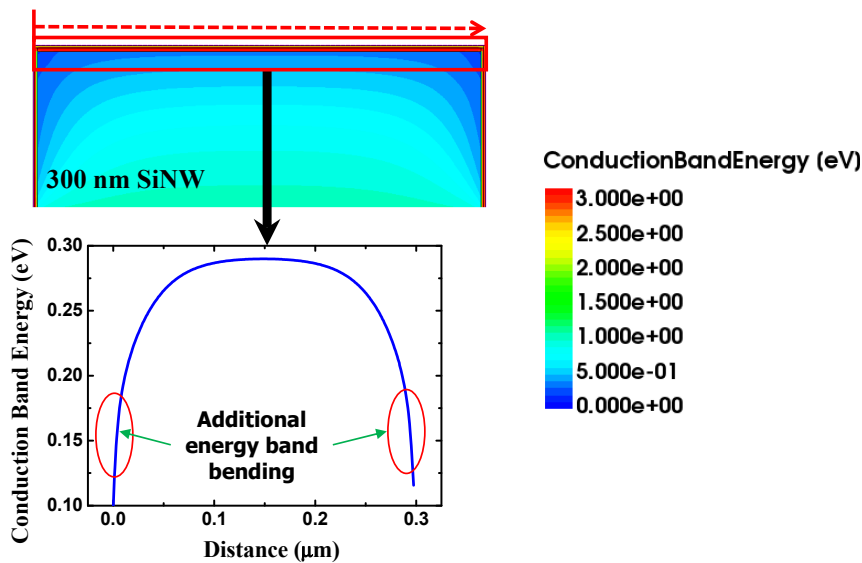


Fig. 8. (Color online) Simulated conduction band energy along the surface of 300 nm SiNW.

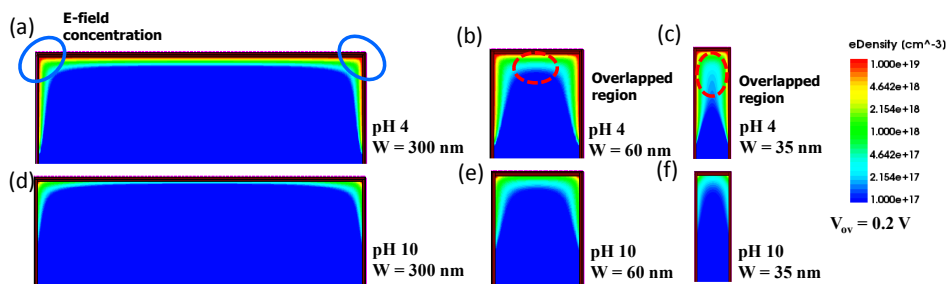


Fig. 9. (Color online) Simulated cross-sectional electron density extracted from SiNWs with widths of (a), (d) 300 nm; (b), (e) 60 nm; and (c), (f) 35 nm.

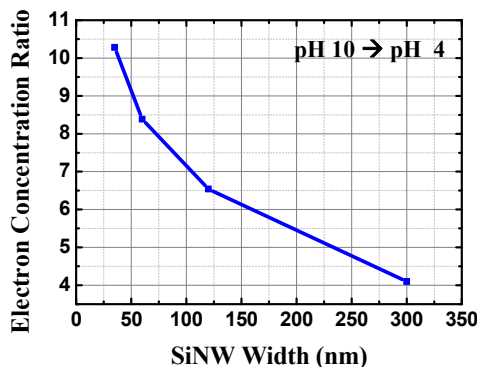


Fig. 10. (Color online) Extracted ratio of electron concentration at pH 4 to that at pH 10 by integrating simulated electron density in Fig. 9.

centrated. On the other hand, as the nanowire gets narrower “under 60 nm”, each side of the region with the concentrated e-field begins to interact and overlap as shown in Fig. 9. As a result, the top area of the channel is more easily activated by the accumulated electrons and the relative increase in the number of accumulated electrons in the SiNW is enhanced. Therefore, sensitivity enhancement in narrow SiNW is due to the increase in surface-to-volume ratio as well as the overlap of e-field concentrated regions. This tendency can be explained by the additional effect of the overlap of the e-field concentrated regions. Furthermore, it is found that the effect of increasing surface-to-volume ratio declines with decreasing SiNW width. In Fig. 11(b), the rate of sensitivity increase gradually decreases as surface-to-volume ratio increases

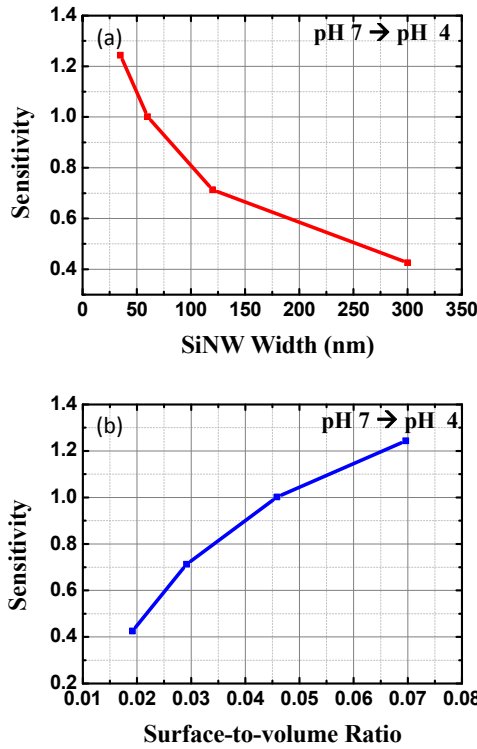


Fig. 11. (Color online) Sensitivity extracted from experimental data at various (a) widths and (b) surface-to-volume ratios as a response of pH change (7 → 4).

(that is, the nanowire width decreases). When only the nanowire width is reduced, the increase in sensitivity owing to the surface-to-volume ratio is limited because the bottom part of the SiNW is difficult to activate with electrons at the given height of SiNW (80 nm).

To summarize, the sensitivity increases and the increase becomes larger as the width of the SiNW decreases, because the effect of concentrated e-fields is added to the existing effect of increasing surface-to-volume ratio, which means that narrower SiNWs have a stronger response to external target ions.

3.2 Length dependence on sensitivity of SiNW sensor

The channel length dependence on sensitivity is investigated. Figure 12(a) shows the measured transfer curves of the SiNWs of various lengths. In general, channel length has a negligible effect on the performance of long-channel ISFETs with a length of more than 1 μm.³¹⁾ However, as shown in Fig. 12(b), it is found that the sensitivity (relative I_{ON} change at a gate overdrive voltage of 0.2 V) increases as the length of the SiNW increases. This trend can be explained by the fact that the parasitic resistance, including source/drain (S/D) resistance, is decreased in the SiNWs with longer channels.³²⁾ The sensitivity (S) examined in this paper can also be expressed as

$$S = \frac{\Delta I}{I} = \frac{I - I_{pH7}}{I_{pH7}} = \frac{\frac{1}{R} - \frac{1}{R_{pH7}}}{\frac{1}{R_{pH7}}} = \frac{R_{pH7} - R}{R} = \frac{-\Delta R_{nw}}{R_S + R_{nw} + R_d} \quad (1)$$

Here, R_S and R_d denote the resistances of the source and drain, respectively. R_{nw} denotes the intrinsic channel resistance of the ISFET. When H^+ or OH^- ions are attached to the gate oxide, the channel resistance (ΔR_{nw}) changes. Note that

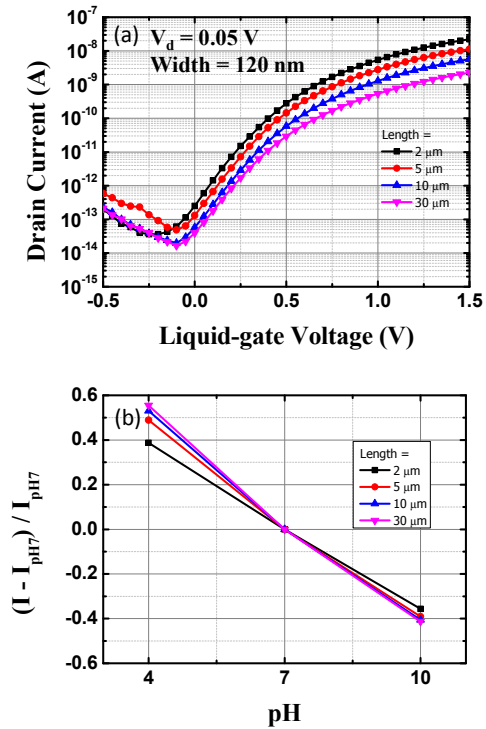


Fig. 12. (Color online) (a) Transfer curves of n-type SiNW ISFETs of various lengths measured at pH 7 and (b) I_{ON} sensitivity of ISFETs of various lengths.

both R_{nw} and ΔR_{nw} increase as the channel length increases. As the ISFET channel length increases, R_{nw} increases and becomes a major part of the total resistance of the ISFET. Since R_S and R_d extracted from Fig. 13 remain constant in Eq. (1), the relative resistance change (S) in Eq. (1) according to pH variations increases as the SiNW becomes longer. Furthermore, it is predictable from Eq. (1) that the extent of increase in sensitivity is gradually reduced with increasing channel length because R_S and R_d make up a smaller proportion of the total resistance and finally become negligible. Figure 14 shows the extracted sensitivity ($\Delta I_{ON}/I_{ON}$ at pH 7) compared with the relative nanowire resistance change ($\Delta R_{nw}/R_{nw}$). The nanowire resistances are extracted by removing S/D parasitic resistances (extracted from Fig. 13) from the total resistance (I_{ON}/V_d) of the ISFET. It is clearly observed that S increases with increasing nanowire length and saturates when the nanowire length exceeds about 10 μm. On the other hand, the relative change in SiNW resistance ($\Delta R_{nw}/R_{nw}$) is almost unchanged as the SiNW length varies. This phenomenon implies that the sensitivity dependence on SiNW length is mainly affected by S/D parasitic resistances. In addition, the effect of S/D resistances is diminished in longer SiNW channels and finally the correlation between SiNW length and sensitivity disappears.

Consequently, the sensitivity resulting from the relative I_{ON} change is improved as the channel length increases owing to the decreased influence of R_S and R_d . However, the sensitivity improvement by using longer channels is limited up to approximately 10 μm as the influence of R_S and R_d decreases in longer SiNWs.

4. Conclusions

We have researched the sensitivity trend of SiNW ISFET-

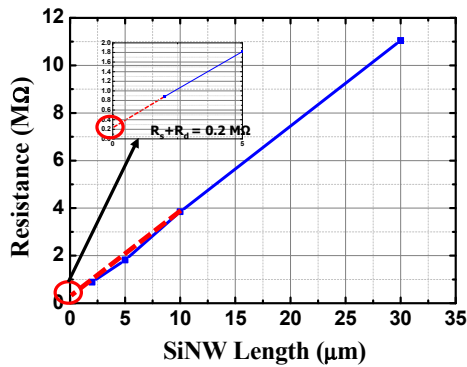


Fig. 13. (Color online) Extraction of source and drain resistances from output curves.

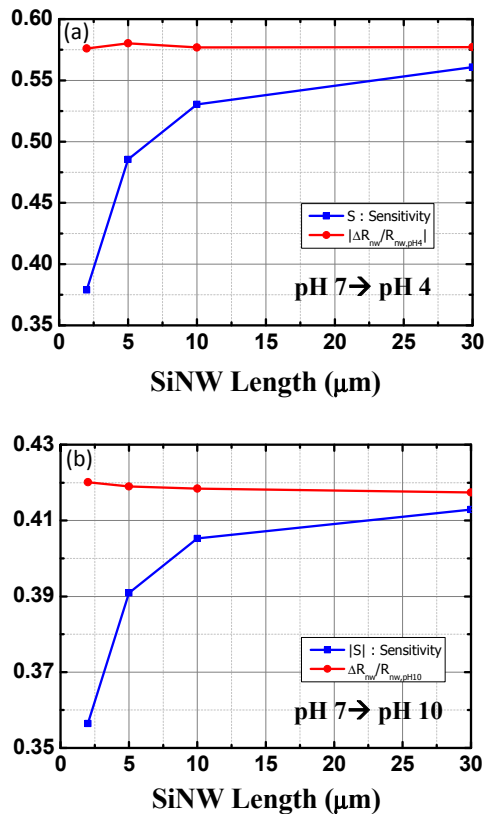


Fig. 14. (Color online) Relationship between the ratio of change of nanowire resistance ($\Delta R_{nw}/R_{nw}$) and sensitivity at various lengths in (a) pH 4 and (b) pH 10 solutions.

based pH sensors of various widths and lengths. From the experimental results, it is estimated that SiNWs with smaller widths have a greater relative on-current change at a fixed gate voltage and thus have higher sensitivity than those with larger widths. Through TCAD simulations, it is verified that the SiNWs with smaller widths have higher accumulated carrier concentration inside the channel in response to pH variations owing to the overlap of electric field concentrated regions. Furthermore, the relationship between the sensitivity and length of SiNW is successfully supported by the obtained experimental data. The sensitivity is improved as the length of SiNWs increases because the source/drain resistances occupy a smaller proportion of the total resistance. Therefore, the use of narrower and longer ISFETs will improve the sensing performance of SiNW ISFETs.

Acknowledgments

This work was supported by the Brain Korea 21 Plus Project in 2017, in part by the Future Semiconductor Device Technology Development Program (Grant 10067739) funded by MOTIE (Ministry of Trade, Industry & Energy) and KSRC (Korea Semiconductor Research Consortium), and in part by the National Research Foundation of Korea (NRF) funded by the Korean Government under Grant Numbers 2013R1A1A2065339, 2016R1A5A1012966, and 2016R1A6A3A01006588.

- 1) G.-J. Zhang and Y. Ning, *Anal. Chim. Acta* **749**, 1 (2012).
- 2) K.-I. Chen, B.-R. Li, and Y.-T. Chen, *Nano Today* **6**, 131 (2011).
- 3) Z. Li, Y. Chen, X. Li, T. I. Kamins, K. Nauka, and R. S. Williams, *Nano Lett.* **4**, 245 (2004).
- 4) M. M.-C. Cheng, G. Cuda, Y. L. Bunimovich, M. Gaspari, J. R. Heath, H. D. Hill, C. A. Mirkin, A. J. Nijdam, R. Terracciano, T. Thundat, and M. Ferrari, *Curr. Opin. Chem. Biol.* **10**, 11 (2006).
- 5) N. C. Tansil and G. Zhiqiang, *Nano Today* **1**, 28 (2006).
- 6) I. Park, Z. Li, A. P. Pisano, and R. S. Williams, *Nanotechnology* **21**, 015501 (2010).
- 7) M. A. Mohd Azmi, Z. Tehrani, R. P. Lewis, K.-A. D. Walker, D. R. Jones, D. R. Daniels, S. H. Doak, and O. J. Guy, *Biosens. Bioelectron.* **52**, 216 (2014).
- 8) M. Y. Shen, B. R. Li, and Y. K. Li, *Biosens. Bioelectron.* **60**, 101 (2014).
- 9) A. Gao, N. Lu, Y. Wang, P. Dai, T. Li, X. Gao, Y. Wang, and C. Fan, *Nano Lett.* **12**, 5262 (2012).
- 10) E. Stern, J. F. Klemic, D. A. Routenberg, P. N. Wyrembak, D. B. Turner-Evans, A. D. Hamilton, D. A. LaVan, T. M. Fahmy, and M. A. Reed, *Nature* **445**, 519 (2007).
- 11) P. Ginet, S. Akiyama, N. Takama, H. Fugita, and B. Kim, *J. Micromech. Microeng.* **21**, 065008 (2011).
- 12) A. Kim, C. S. Ah, H. Y. Yu, J.-H. Yang, I.-B. Baek, C.-G. Ahn, C. W. Park, M. S. Jun, and S. Lee, *Appl. Phys. Lett.* **91**, 103901 (2007).
- 13) Y. Cui, Q. Wei, H. Park, and C. M. Lieber, *Science* **293**, 1289 (2001).
- 14) J. Lee, B. Choi, S. Hwang, J. H. Lee, B.-G. Park, T. J. Park, D. M. Kim, D. H. Kim, and S.-J. Choi, *IEEE Trans. Electron Devices* **61**, 1607 (2014).
- 15) P. R. Nair and M. A. Alam, *IEEE Trans. Electron Devices* **54**, 3400 (2007).
- 16) K. Shoorideh and C. O. Chui, *Proc. Natl. Acad. Sci. U.S.A.* **111**, 5111 (2014).
- 17) L. Bousse, N. F. De Rooij, and P. Bergveld, *IEEE Trans. Electron Devices* **30**, 1263 (1983).
- 18) J. Bausells, J. Carrabina, A. Errachid, and A. Merlos, *Sens. Actuators B* **57**, 56 (1999).
- 19) Y.-L. Chin, J.-C. Chou, T.-P. Sun, H.-K. Liao, W.-Y. Chung, and S.-K. Hsiung, *Sens. Actuators B* **75**, 36 (2001).
- 20) P. R. Nair and M. A. Alam, *Appl. Phys. Lett.* **88**, 233120 (2006).
- 21) W. Lu, P. Xie, and C. M. Lieber, *IEEE Trans. Electron Devices* **55**, 2859 (2008).
- 22) N. Yang, X. Chen, T. Ren, P. Zhang, and D. Yang, *Sens. Actuators B* **207**, 690 (2015).
- 23) J.-H. Ahn, S.-J. Choi, J.-W. Han, T. J. Park, S. Y. Lee, and Y.-K. Choi, *IEEE Trans. Nanotechnol.* **10**, 1405 (2011).
- 24) X. Yang, W. R. Frensley, D. Zhou, and W. Hu, *IEEE Trans. Nanotechnol.* **11**, 501 (2012).
- 25) K.-S. Shin, A. Pan, and C. O. Chui, *Appl. Phys. Lett.* **100**, 123504 (2012).
- 26) J. Lee, S. Hwang, B. Choi, J. H. Lee, D.-I. Moon, M.-L. Seol, C.-H. Kim, I.-Y. Chung, B.-G. Park, Y.-K. Choi, D. M. Kim, D. H. Kim, and S.-J. Choi, *IEDM Tech. Dig.*, 2013, p. 385.
- 27) J. Lee, J.-M. Lee, J. H. Lee, W. H. Lee, M. Uhm, B.-G. Park, D. M. Kim, Y.-J. Jeong, and D. H. Kim, *IEEE Electron Device Lett.* **33**, 1768 (2012).
- 28) B. Choi, J. Lee, J. Yoon, J.-H. Ahn, T. J. Park, D. M. Kim, D. H. Kim, and S.-J. Choi, *IEEE Trans. Electron Devices* **62**, 1072 (2015).
- 29) R. A. Chapman, P. G. Fernandes, H. J. Stiegler, H.-C. Wen, Y. J. Chabal, and E. M. Vogel, *IEEE Trans. Electron Devices* **58**, 1752 (2011).
- 30) A. Ortiz-Conde, F. J. Garcia Sanchez, J. J. Liou, A. Cerderia, M. Estrada, and Y. Yue, *Microelectron. Reliab.* **42**, 583 (2002).
- 31) Y. Taur and T. H. Ning, *Fundamentals of Modern VLSI Devices* (Cambridge University Press, Cambridge, U.K., 2009) 2nd ed.
- 32) L. Zeimpekis, K. Sun, C. Hu, O. Thomas, M. R. De Planque, H. M. Chong, H. Morgan, and P. Ashburn, *Nanoscale Res. Lett.* **10**, 79 (2015).